Journal of Solid State Chemistry 182 (2009) 875–880

Contents lists available at ScienceDirect

Journal of Solid State Chemistry

journal homepage: www.elsevier.com/locate/jssc

A simple route to synthesize carbon-nanotube/cadmium-sulfide hybrid heterostructures and their optical properties

Yongbin Zhao [a,b], Haijing Liu [a,b], Feng Wang [a,b,*], Jingjun Liu [a,b], Ki Chul Park [c], Morinobu Endo [c]

[a] State Key Laboratory of Chemical Resource Engineering, Beijing University of Chemical Technology, Beijing 100029, PR China
[b] Institute of Carbon Fibers and Composites, Beijing University of Chemical Technology, Beijing 100029, PR China
[c] Department of Electrical and Electronic Engineering, Faculty of Engineering, Shinshu University, 4-17-1 Wakasato, Nagano-shi, Nagano 380-8553, Japan

ARTICLE INFO

Article history:
Received 28 August 2008
Received in revised form
29 December 2008
Accepted 1 January 2009
Available online 9 January 2009

Keywords:
CdS nanoparticles
Semiconductor compounds
Carbon and graphite
Nanocomposites
Optical spectroscopes

ABSTRACT

Multi-walled carbon nanotube/cadmium sulfide hybrid heterostructures were easily synthesized by employing a thermal decomposition of thioacetamide as a sulfide-ion source in an aqueous regime. The resulting cadmium-sulfide phase is comprised of a zinc-blende structure of spherical polycrystalline nanoparticles (cadmium-sulfide nanoclusters) with the subunits of ca. 15 nm, deposited on the nanotube surface. The formation of the cadmium-sulfide nanoparticles with zinc-blende structure (cubic crystal) suggests that the local concentrations of reacting ion species in the vicinity of the nanotube surface are different from those in the reaction solution. The cadmium-sulfide nanoparticles are comprised of a stoichiometrically ideal chemical-composition ratio (cadmium: sulfur = 1:1.02) of cadmium and sulfur with the valence states of +2 and −2, respectively. The optical responses of the cadmium-sulfide phase for ultraviolet-visible light and photoluminescence spectroscopes show the proper size-effect and inherent optical properties of the cadmium-sulfide nanoparticles.

1. Introduction

Multi-walled carbon nanotubes (MWCNTs) have been widely applied as a promising raw material in many areas of science and technology due to their outstanding physical and electrical properties such as high tensile strength and elastic modulus and excellent thermal and electrical conductivity [1–4]. So far, MWCNTs have been used to synthesize not only various composite materials mainly including polymer/MWCNT [5] and metal/MWCNT [6,7] composites but also various MWCNT/metal-nanoparticle hybrid catalysts, where the MWCNTs can function as supporting materials [8].

The decoration of carbon nanotubes (CNTs) with organic or inorganic compounds through covalent and non-covalent bonds can give them new properties and potentials for various new applications. Among these, the CNTs modified with nanocrystalline semiconductor particles are more active due to their size-dependant nonlinear optical, physical and electronic properties, which make them to be promising materials and provide potentials of their application in several fields [9–17]. Thus far, several semiconductor nanoparticles such as CdSe/ZnS [11], CdTe [12], CdSe [13], ZnS [14], PbSe [15] and CdS [16–19] have been bound to the surface of CNTs.

The difference in the preparation methods of the hybrid materials provides the different morphology and structure of semiconductors on/into CNTs [16–21]. As for CdS, thiol groups pre-introduced into CNTs have cadmium ions (Cd^{2+}) attached onto the nanotube surface, so that the simple mixing with sulfide ions (S^{2-}) has provided the coating of CdS nanoparticles [16]. Instead of the covalently introduced binding sites of Cd^{2+}, the use of an organic linker molecule has successfully deposited well-isolated CdS nanoparticles with cubic phase onto the nanotube surface by the simple addition of S^{2-} [17]. On the other hand, in-situ formation of S^{2-} by the chemical reduction of S has deposited a beplastered and uniform layer of CdS with hexagonal phase [21]. Other methods for preparing CNT/CdS hybrid materials include thermally induced processes. The difference of reaction regimes (e.g., solvent, reaction duration, and reactant concentration) in thermal processes has also provided different morphology and structure of CdS on the surface of CNTs [18,19]. These reports demonstrate well that the combination between CNTs and other different preparation methods of CdS has a possibility to form different types of CNT/CdS hybrid materials.

Libert et al. previously reported the synthesis of the uniform colloidal cadmium sulfide (CdS) spheres, which are formed by precipitation in an acidic aqueous solution during the thermally controlled reaction between cadmium nitrate and thioacetamide (TAA) [22,23]. We report here an easy synthesis route of CNT/CdS

* Corresponding author at: Institute of Carbon Fibers and Composites, Beijing University of Chemical Technology, Beijing 100029, PR China.
Fax: +86 10 64411301.
E-mail address: wangf@mail.buct.edu.cn (F. Wang).

0022-4596/$ - see front matter © 2009 Elsevier Inc. All rights reserved.
doi:10.1016/j.jssc.2009.01.001

hybrid heterostructures, which is achieved by employing a thermal decomposition method of TAA as a sulfide-ion source. Furthermore, we discuss the structure, shape and optical properties of the CNT/CdS hybrid materials, as well as the deposition state of CdS phase on the CNT surface.

2. Experimental

2.1. Materials

All solvents and chemicals (analytical reagent quality) were obtained commercially and used without purification. The MWCNTs used in the present study were synthesized by a catalyst-assisted chemical vapor deposition (CVD) method [24]. Then, the products were thermally treated at 2800 °C under an argon flow for 30 min for graphitization.

2.2. Synthesis

MWCNTs (100 mg) were stirred in 40 mL of 0.1 M hydrochloric acid (HCl) aqueous solution for 5 h at room temperature to remove residual catalyst nanoparticles. The purified MWCNTs were treated by nitric-sulfuric acid (HNO_3–H_2SO_4, volumetric ratio: v/v = 1/3) solution for 24 h at room temperature, according to the literature [25]. Then, the reaction mixture was filtrated, and washed well with deionized water to remove the remaining acid. The acid-treated MWCNTs can be easily suspended in water due to the relatively large amount of surface-bounded carboxyl-acid groups.

MWCNT/CdS heterostructure materials were prepared through the reaction of cadmium sulfate ($CdSO_4$) with S^{2-} resulting from the thermal decomposition of TAA in the presence of MWCNTs in aqueous solution. A typical synthesis is as follows: MWCNTs (100 mg) were dispersed by sonication in 25 mL of H_2O. On the other hand, $3CdSO_4.8H_2O$ (25.6 mg, 0.0726 mmol) was dissolved in 10 mL of H_2O, and TAA (82.5 mg, 1.098 mmol) was dissolved in 10 mL of H_2O. Then the suspension of the MWCNTs and the two solutions were mixed, and stirred at 80 °C for 6 h. The obtained black precipitate was filtered, washed with distilled water, and dried in a vacuum at 80 °C for 10 h (dry weight of the product: 115.6 mg). In this experiment, the excess molar amount of TAA was employed for Cd^{2+}. The ideal loading of CdS calculated from the expected weight increase and the initial weight of MWCNTs is 31.4%. However, the actual loading of CdS was 15.6%. The difference between the ideal and actual loadings might be caused by the loss of CdS nanoparticles non-immobilized on the nanotube surface during filtration.

2.3. Characterization

Powder X-ray diffraction (XRD) patterns were obtained on a MAC Science MX Labo2 X-ray diffractometer equipped with graphite monochromatized Cu $K\alpha$ radiation ($\lambda = 1.541874$ Å). The acceleration voltage was set at 35 kV with a 25 mA flux. The scanning rate was 0.04°/s in the 2θ range of 10–90°. The Fourier-transform infrared (FT-IR) spectra were recorded on a MAGNA-IR 750 FT-IR spectrometer using a KBr-disc method. X-ray photoelectron spectroscopy (XPS) measurements were conducted using a Thermo Electron ESCALAB250 photoelectron spectrometer. The transmission electron microscopy (TEM) studies were carried out on a Hitachi Model H-800 apparatus with an acceleration voltage of 200 kV. The high-resolution transmission electron microscopy (HR-TEM) images were obtained on a JEOL-2010 transmission electron microscope. The morphological features of the hybrid materials were observed using S-4700 field-emission scanning electron microscope. The ultraviolet and visible light (UV–vis) spectra were recorded on a Shimadzu UV-3150 UV–vis-near infrared (NIR) spectrophotometer. The photoluminescence (PL) spectra were obtained on a CARY Eclipse fluorescence spectrophotometer.

3. Results and discussion

3.1. Pretreatment of CNTs

The SEM images of Fig. 1a show that the as-prepared MWCNTs have a diameter of 100–200 nm and a length of several microns to

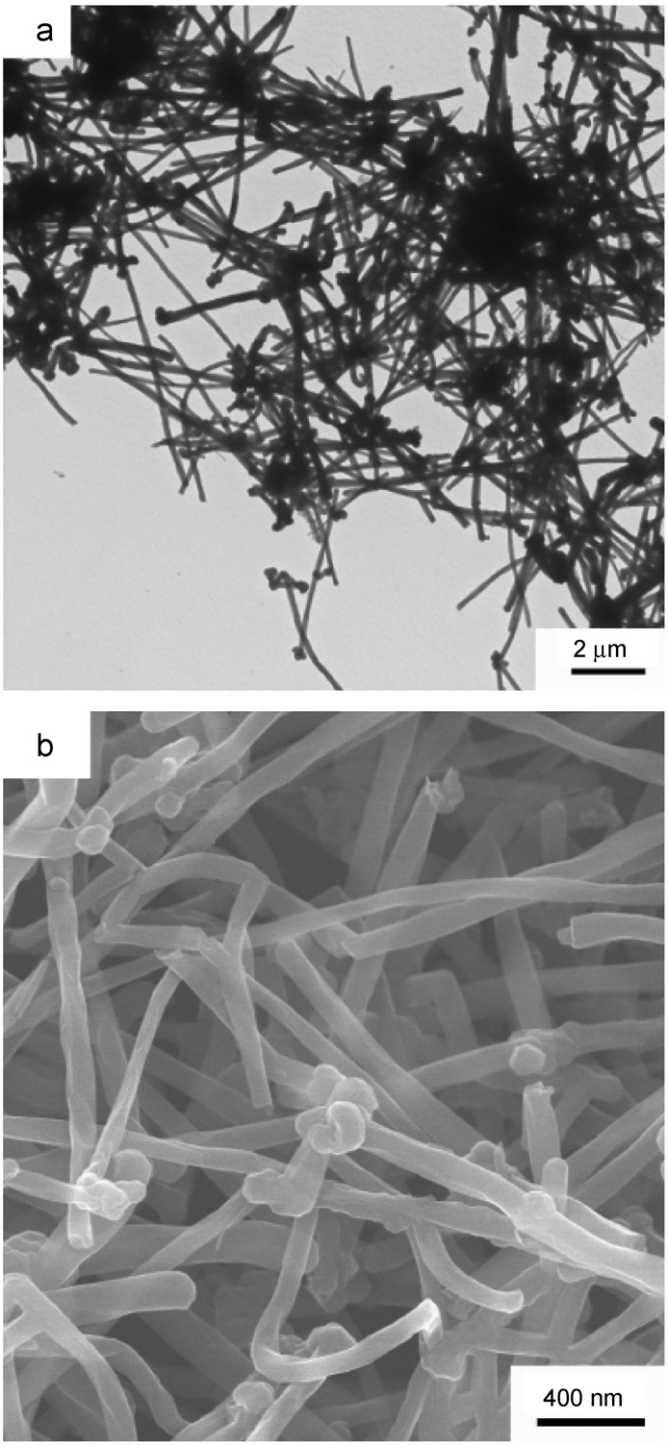

Fig. 1. TEM image of the pristine MWCNTs and SEM image of the acid-treated MWCNTs.

several tens of microns. As can be seen from Fig. 1b, after purified by HCl solution and acid-oxidized by HNO_3–H_2SO_4 mixed solution, residual catalyst nanoparticles have been removed absolutely, while the surface of the acid-pretreated MWCNTs remains smooth.

3.2. Formation of MWCNT/CdS heterostructures

The MWCNT/CdS heterostructure materials were prepared through the reaction of $CdSO_4$ with S^{2-} resulting from the thermal decomposition of TAA in the presence of MWCNTs in aqueous solution. The TEM (Fig. 2a) and SEM (Fig. 2c and d) observations have ensured the success of the attachment of CdS nanoparticles onto CNTs. Clearly, CdS nanoparticles are deposited on the surface of CNTs. The electron diffraction pattern (in Fig. 2b) shows the reflection of zinc blende crystal structure corresponding to (111) planes of cubic CdS phase, in addition to the reflection of the (002) planes of CNT graphite. Furthermore, the CdS nanoparticles with the size of several tens to hundreds nanometer proved to be composed of the smaller nanoparticles (subunits) with the size of about 10–20 nm (Fig. 2d), which is consistent with the values calculated using Scherrer equation (see below).

In this work, TAA was employed as a weak sulfide source, which was previously used for the control of nucleation and growth directing the shape of zinc sulfide [26]. The formation of uniform colloidal CdS spheres proceeds according to the following equations [14]:

$$C_2H_5NS \rightarrow S^{2-} + \text{byproducts} \quad (1)$$

$$Cd^{2+} + S^{2-} \rightarrow CdS\ (\text{solute}) \quad (2)$$

$$n\text{CdS} \rightarrow (\text{CdS})n\ (\text{solid}) \quad (3)$$

The step 1 is a rate-determining reaction for availability of CdS solute species due to the relatively slow release of S^{2-} by the temperature-dependent decomposition of TAA [22,23]. At a given concentration of TAA, the concentration of S^{2-} depends on the acidity of the solution and the reaction time. The sizes of the crystalline subunits and the final CdS particles are affected by the concentration ratio of $[Cd^{2+}]/[S^{2-}]$. The lower $[Cd^{2+}]/[S^{2-}]$ ratio corresponds to the faster release rate of S^{2-}, which results in

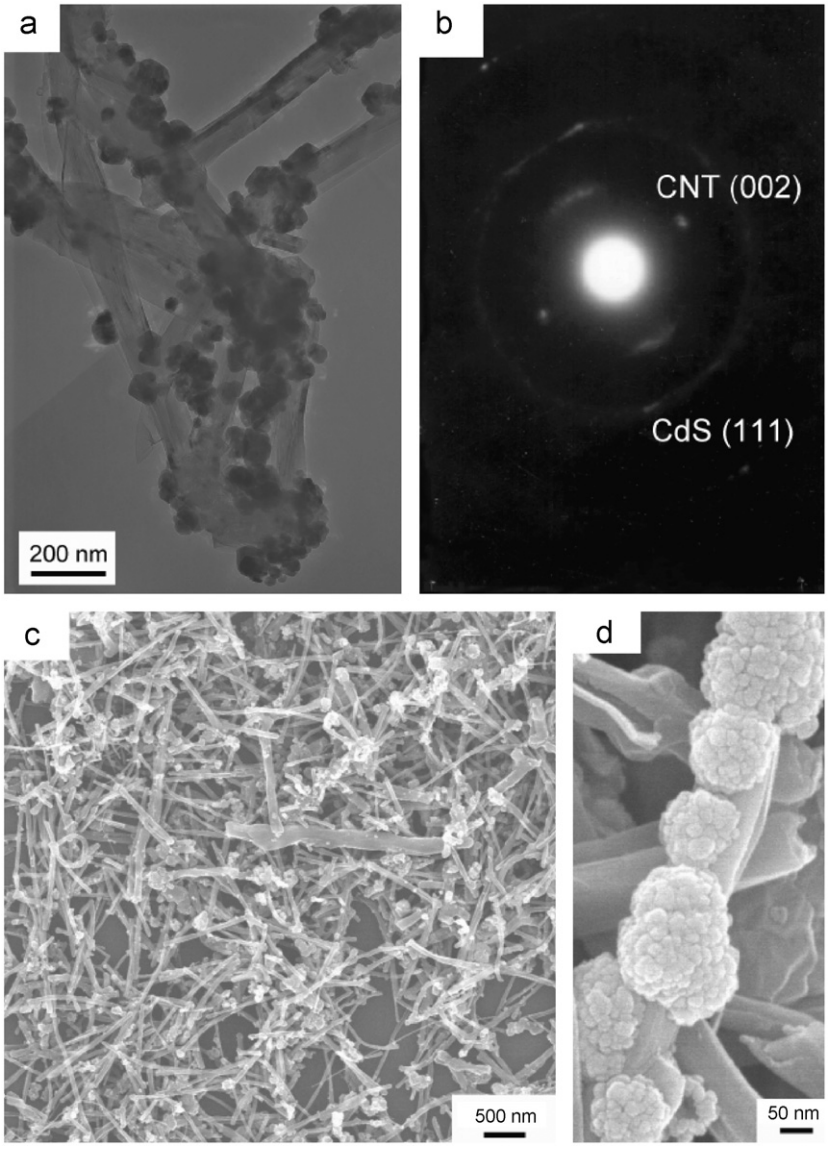

Fig. 2. TEM and SEM images of the MWCNT/CdS heterostructures.

the formation of greater number of primary particles. The higher concentration of the primary particles yields a greater number of clustering centers, leading to the formation of smaller size of final CdS particles. Furthermore, the lower concentration ratio prompts the formation of hexagonal crystal lattice, while the higher concentration ratio gives the partial cubic crystal lattice. The release rate of S^{2-} is dependent on the concentration of TAA in the reaction solution. Thus, we employed the excess molar amount of TAA (1.098 mmol) for $CdSO_4$ (0.0726 mmol) in order to give a low $[Cd^{2+}]/[S^{2-}]$ ratio during the reaction. Furthermore, the heating condition of 80 °C employed in this work is considered to afford relatively fast decomposition rate of TAA, i.e., the fast release rate of S^{2-} [14]. Therefore, the smaller sizes of the crystalline subunits and the final particles are expected at the reaction temperature of 80 °C. However, the adsorption and desorption of Cd^{2+} ions on the CNT surface would be affected by the oxygen-containing functional groups (such as –C(=O)OH groups) of the CNT surface [27] and the surface charges of electric double layers formed in the aqueous solution. This would lead to the possibility that concentration gradient of the Cd^{2+} ions occurs between on the CNT surface and in the reaction solution. The presence of the $[Cd^{2+}]$ gradient on the CNT surface might change a local $[Cd^{2+}]/[S^{2-}]$ ratio in the vicinity of CNTs to make the formation manner of CdS particles and the crystal lattice structure different from that proceeding in the simple solution reaction. Although the local concentration ratio is unknown, the results of this work imply that the continuous surface reaction of Cd^{2+} ions with free S^{2-} would form the primary particles of CdS, which further grow to the final CdS particles on the CNT surface. Moreover, the abundant surface groups of CNTs would enrich locations for the deposition of CdS particles by acting as effective anchor sites.

3.3. Structural characterization

Fig. 3a shows the XRD patterns of the pristine MWCNTs. The peaks centered at 26° and 44° correspond to the (002) and (100) reflections of graphite from the CNTs, respectively [7]. The acid-oxidized CNTs (Fig. 3b) also show the (002) and (100) reflections similar to those of the pristine MWCNTs. The XRD patterns of MWCNT/CdS heterostructures (Fig. 3c) and a bulk sample of pure CdS nanoparticles (Fig. 3d) gave the peaks assigned to the (111), (200), (220), (311), and (222) phase of the cubic CdS crystal structure of zinc blende, which are in good agreement with the reported data for CdS (JCPDS Card File,89-0440), though the (002) peak of CNTs is overlapped with the (111) peak of the cubic CdS. The results demonstrate that the cubic CdS crystal structure of zinc blende is formed on the surfaces of CNTs, which agrees well with the electron diffraction pattern discussed above. The average size of CdS subunits was determined from the width of the reflection according to Scherrer equation [25]. The mean subunit-size calculated by the (220) reflection was ca. 15 nm. The size is much smaller than the particle size (several tens to several hundreds nm) estimated by the SEM and TEM observations. It is therefore concluded that the CdS nanoparticles (CdS nanoclusters) are composed of the smaller crystals (subunits) with the size of 15 nm. As mentioned above, the $[Cd^{2+}]/[S^{2-}]$ ratio affects the crystal-lattice structure of CdS nanoparticles [14]. In this work, the excess molar amount of TAA for $CdSO_4$ was employed in order to lower the $[Cd^{2+}]/[S^{2-}]$ ratio during the reaction. Therefore, we had predicted the formation of CdS phase with hexagonal crystal lattice. However, the obtained CdS nanoparticles are comprised of not hexagonal but cubic crystal structure. This suggests that the local concentrations of reacting ion species on the CNT surface are different from those in the reaction solution, i.e., the local $[Cd^{2+}]/[S^{2-}]$ ratio in the vicinity of the CNT surface would be higher than that of the surrounding solution.

The chemical state of the CNT surface was characterized by FT-IR spectroscopy. As seen from the comparison between Fig. 4a and b, the modification of the CNT surface by the HNO_3–H_2SO_4 mixed acid gives a newly developing absorption peak at 1730 cm^{-1}, which is assigned to carboxyl C=O groups [28]. The intensive peak at 3450 cm^{-1} and the peak at 1630 cm^{-1}, observed in every spectrum, originate from the absorption of water by KBr matrix (3450 and 1630 cm^{-1}: stretching and deformation vibrations of H_2O, respectively). The existence of the water-induced absorption peak makes the expectable peak of carboxyl –OH vibration invisible. Note that the absorption peak at 1730 cm^{-1} clearly becomes weakening for the MWCNT/CdS heterostructures (Fig. 4c). This indicates that the CdS deposition is achieved on the carboxyl groups of the CNT surface, which would act as anchoring sites of the CdS nanoparticles.

Fig. 5 shows the C1*s*, Cd3*d* and S2*p* regional XPS spectra of the MWCNT/CdS heterostructures, all of which were referenced to the C1*s* peak (binding energy: BE = 284.6 eV) [29] arising from sp^2-hybridized carbon of CNTs. The regional spectrum of C1*s* displays

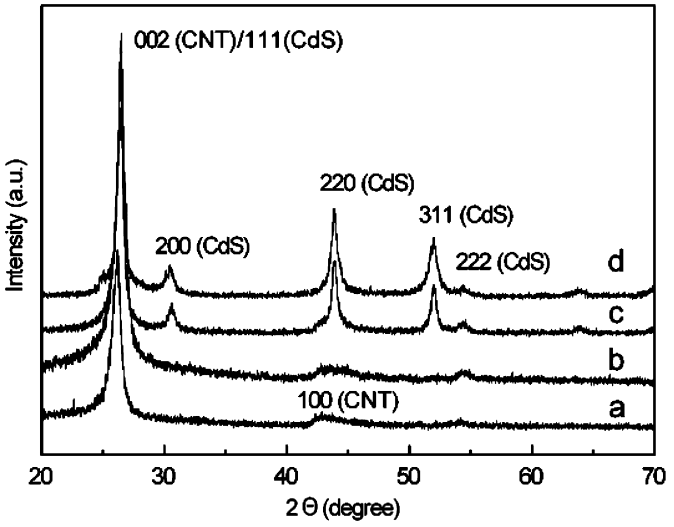

Fig. 3. XRD patterns of: (a) the pristine MWCNTs, (b) the acid-oxidized MWCNTs, (c) the MWCNT/CdS heterostructures and (d) bulk CdS nanoparticles.

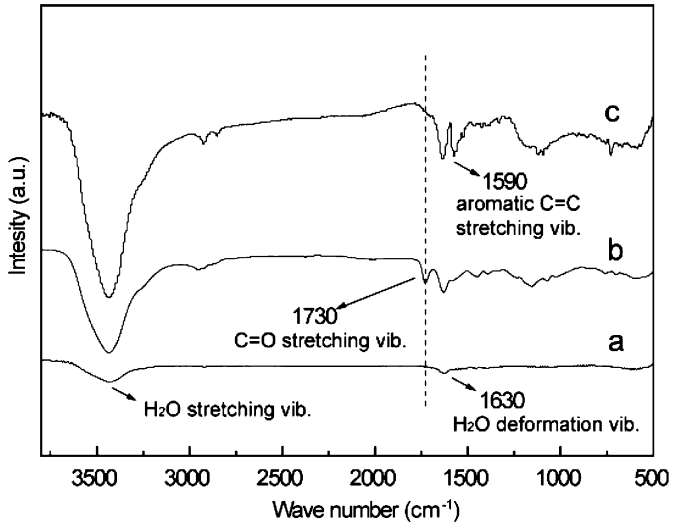

Fig. 4. FT-IR spectra of: (a) the pristine MWCNTs, (b) the acid-oxidized MWCNTs and (c) the MWCNT/CdS heterostructures.

an asymmetrical intensive peak and a very broad peak in the baseline, as shown in Fig. 5a. The deconvolution of the C1*s* peaks indicates the presence of two peaks at 286.3 and 288.8 eV other than the main peak of sp^2-carbon at 284.6 eV. The peaks at 286.3 and 288.8 eV can be attributed to hydroxyl carbon (C–OH) and carboxyl carbon (O═C–O) on the CNT surface, respectively. The results indicate that the carboxyl-acid groups are introduced into the CNT surface by the oxidation with HNO_3–H_2SO_4 mixed acid, which is consistent with that of the FT-IR analysis. The regional spectra of Cd3*d* and S2*p* (Fig. 5b and c) show pairs of symmetrical peaks with the binding energies of 405.9 eV for Cd3$d_{5/2}$, 412.6 eV for $Cd_{3/2}$, 161.7 eV for S2$p_{3/2}$, and 163.8 eV for S2$p_{1/2}$. The BE values are very close to the reported ones [30], indicating that the valence states of Cd and S are +2 and −2, respectively. Moreover, the quantification of peaks gave a stoichiometrically ideal chemical-composition ratio of Cd:S = 1:1.02, indicating that the CdS is quite pure. As described above, the results of the FT-IR analysis imply that the CdS nanoparticles are attached on the carboxyl-acid groups acting as anchoring sites. However, it will be difficult to observe by XPS analysis the chemical states of CdS anchored on the carboxyl-acid groups because of the large size of the CdS nanoclusters, as is shown by the SEM and TEM analysis.

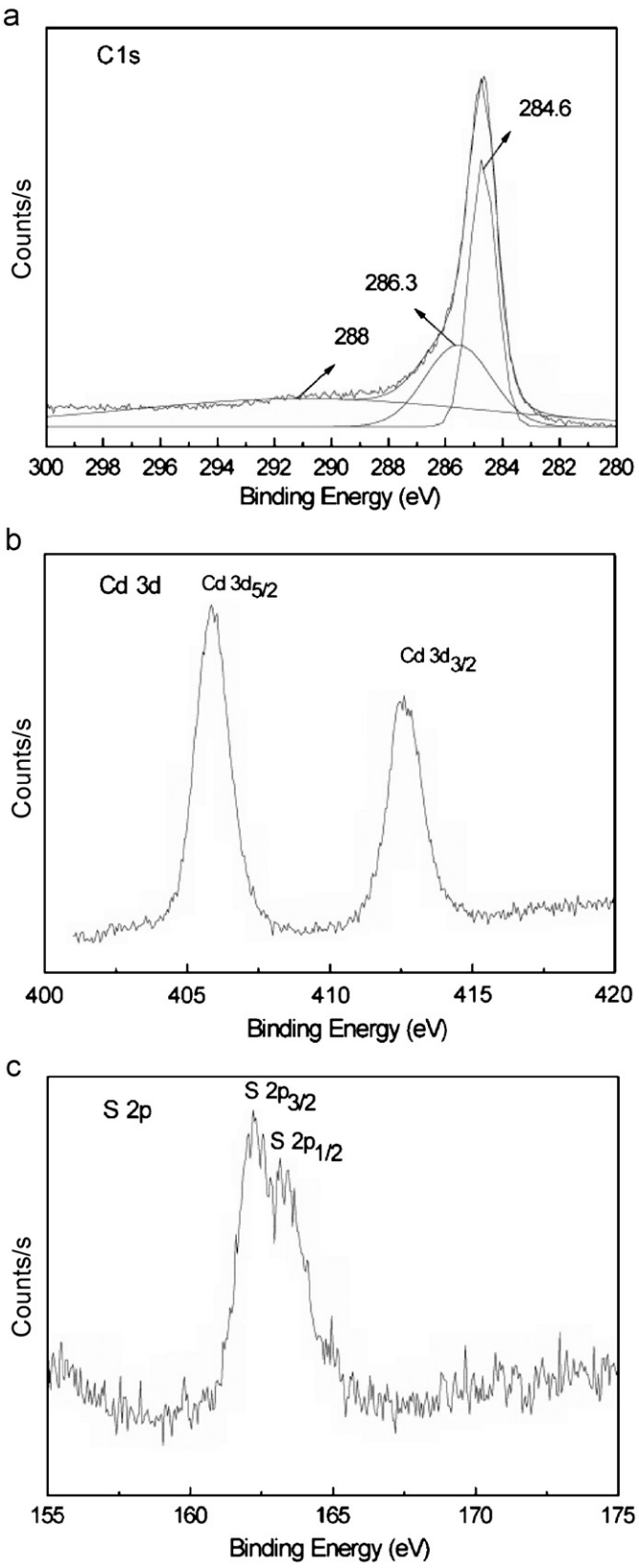

Fig. 5. XPS spectra of the MWCNT/CdS heterostructures.

3.4. Optical proprieties of the MWCNT/CdS heterostructures

The UV–vis absorption spectra of the MWCNT/CdS heterostructures are shown in Fig. 6. The measurements were conducted for dispersions in ethanol at room temperature. The pristine and acid-oxidized MWCNTs gave no specific absorption spectra (Fig. 6a and b). In contrast, the MWCNT/CdS heterostructures show an absorption band of CdS at 520 nm, which shifts to a shorter side of wavelength compared with the characteristic absorption (550 nm) of bulk CdS [31]. The blue shift of the absorption wavelength is probably due to the size effect of the CdS nanoparticles, which is consistent with the previous results [32]. The formation of the CdS nanoparticles on the CNT surface indicates that the growth of CdS is effectively confined in nanometer scale on the CNTs in the synthesis regime. The solid-state PL spectra of the pristine MWCNTs, the acid-oxidized MWCNTs and the MWCNT/CdS heterostructures were shown in Fig. 7, which were obtained by using a 390-nm excitation line. As shown in Fig. 7a and b, the pristine and acid-oxidized MWCNTs gave no specific PL response. In contrast, the MWCNT/CdS heterostructures show an obvious PL peak at 546 nm originating from the band-to-band emission of the CdS nanoparticles, in agreement with the previous report [33].

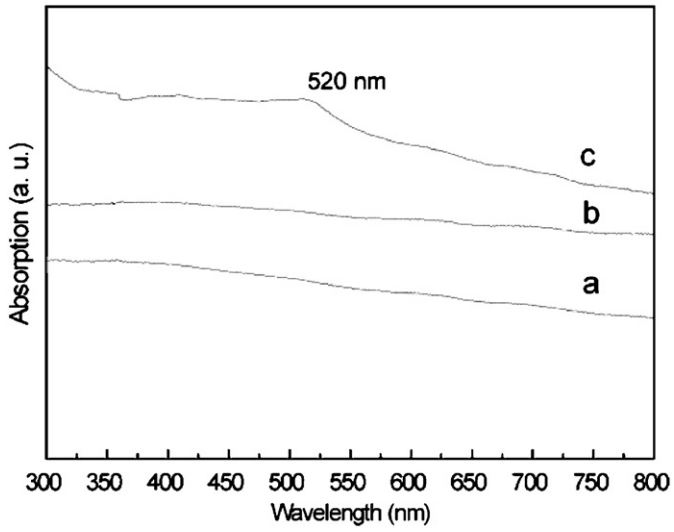

Fig. 6. UV–vis absorption of: (a) the pristine MWCNTs, (b) the acid-oxidized MWCNTs and (c) the MWCNT/CdS heterostructures.

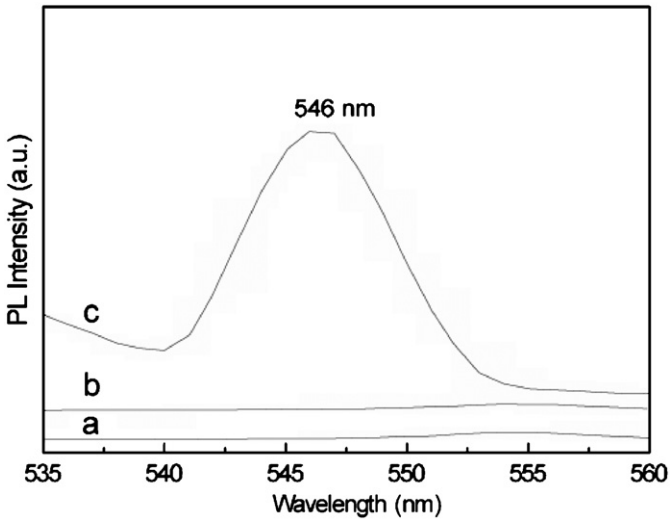

Fig. 7. PL spectra of: (a) the pristine MWCNTs, (b) the acid-oxidized MWCNTs and (c) the MWCNT/CdS heterostructures.

4. Conclusion

The MWCNT/CdS heterostructure materials were easily prepared by a thermal decomposition of TAA in the presence of $CdSO_4$ and CNTs in an aqueous synthesis regime, where the surface reaction between Cd^{2+} and the S^{2-} released through the TAA decomposition achieves the deposition of CdS nanoparticles on the CNT surface. In the present method, the surface modification of CNTs and the sulfide-ion source play an important role in the deposition manner, morphology and structure of the CdS nanoparticles. The XRD, TEM and SEM studies for the MWCNT/CdS heterostructures have revealed that the present synthesis achieves the uniform covering of the CNT surface with a zinc-blende structure of CdS nanoparticles (CdS nanoclusters) comprised of about 15-nm-sized subunits. The formation of the CdS nanoparticles with cubic crystal structure suggests that the local $[Cd^{2+}]/[S^{2-}]$ ratio in the vicinity of the CNT surface are higher than those in the reaction solution. The FT-IR analysis implies that the CdS nanoparticles are deposited on the surface groups of CNTs. Furthermore, the XPS analysis indicates that the CdS nanoparticles consist of a stoichiometrically ideal chemical-composition ratio ($Cd:S = 1:1.02$) of Cd and S with the valence states of +2 and −2, respectively. The UV–vis and PL analyses evidence the proper size-effect and optical properties of the CdS nanoparticles. The results of this work demonstrate that the present method is a promising easy route for synthesizing MWCNT/metal-sulfide heterostructures.

Acknowledgments

The authors acknowledge the financial support from the "863" Project (2006AA05Z202) from the Ministry of Science and Technology of China and Natural Science Foundation of Beijing University of Chemical Technology. This research was partially supported by the Program of Introducing Talents of Discipline to Universities (B08003).

References

[1] R. Andrews, D. Jacques, D. Qian, T. Rantell, Acc. Chem. Res. 35 (2002) 1008–1017.
[2] S. Frank, P. Poncharal, Z.L. Wang, A. Walt, Science 280 (1998) 1744–1746.
[3] P. Kim, L. Shi, A. Majumdar, P.L. McEuen, Phys. Rev. Lett. 87 (2001) 215502-1–215502-2.
[4] S.L. Ruan, P. Gao, X.G. Yang, T.X. Yu, Polymer 44 (2003) 5643–5654.
[5] Y.J. Xu, B. Higgins, W.J. Brittain, Ploymer 46 (2005) 799–810.
[6] F. Wang, S. Arai, M. Endo, Carbon 43 (2006) 1716–1721.
[7] F. Wang, S. Arai, M. Endo, Electrochem. Commun. 7 (2005) 674–678.
[8] S. Banerjee, S.S. Wong, Nano Lett. 2 (3) (2002) 195–200.
[9] M. Olek, T. Büsgen, M. Hilgendorff, M. Ciersig, J. Phys. Chem. B 110 (2006) 12901–12904.
[10] A. Profumo, M. Fagnoni, D. Merli, E. Quartarone, S. Protti, D. Dondi, Anal. Chem. 78 (2006) 4194–4199.
[11] Y.B. Zhao, T.T. Chen, J.H. Zou, W.F. Shi, J. Cryst. Growth 275 (2005) 521–527.
[12] S. Banerjee, S.S. Wong, Adv. Mater. 16 (2004) 34–37.
[13] Y. Yang, H.Y. Wang, X.F. Lu, Y.Y. Zhao, X. Li, X. Wang, Mater. Sci. Eng. B 40 (2007) 48–52.
[14] H. Kim, W. Sigmund, J. Cryst. Growth 255 (2003) 114–118.
[15] N. Cho, K.C. Choudhury, R.B. Thapa, Y. Sahoo, T. Ohulchansky, A.N. Cartwright, Adv. Mater. 19 (2007) 232–236.
[16] Y. Liu, L. Gao, Mater. Chem. Phys. 91 (2005) 365–369.
[17] I. Robel, B.A. Bunker, P.V. Kamat, Adv. Mater. 17 (2005) 2458–2463.
[18] Q. Huang, L. Gao, Nanotechnology 15 (2004) 1855–1860.
[19] B. Liu, J.Y. Lee, J. Phys. Chem. B 109 (2005) 23783–23786.
[20] X. Shen, Z. Jiang, C. Gao, Z. Xu, Z. Xie, L. Zheng, J. Mater. Chem. 17 (2007) 1326–1330.
[21] J. Cao, J.-Z. Sun, J. Hong, H.-Y. Li, H.-Z. Chen, M. Wang, Adv. Mater. 16 (2004) 84–87.
[22] S. Libert, D.V. Goia, E. Matijevic, Langmuir 19 (2003) 10673–10678.
[23] S. Libert, V. Gorshkov, D. Goia, E. Matijevic, V. Privman, Langmuir 19 (2003) 10679–10683.
[24] M. Endo, ChemTech 18 (1988) 568–576.
[25] J.M. Du, L. Fu, Z.M. Liu, B.X. Han, Z.H. Li, Y.Q. Liu, et al., J. Phys. Chem. B 109 (2005) 12772–12776.
[26] Y.B. Zhao, F. Wang, Q. Fu, W.F. Shi, Polymer 48 (2007) 2853–2859.
[27] R. Loscutova, A.R. Barron, J. Mater. Chem. 15 (2005) 4346–4353.
[28] C.S. Li, Y.P. Tang, K.F. Yao, F. Zhou, Q. Ma Q, H. Lin, et al., Carbon 44 (2006) 2021–2026.
[29] J. Li, S.B. Tang, L. Lu, H.C. Zeng, J. Am. Chem. Soc. 129 (2007) 9401–9409.
[30] Z.P. Qiao, G. Xie, J. Tao, Z.Y. Nie, Y.Z. Lin, X.M. Chen, J. Solid State Chem. 166 (2002) 49–52.
[31] K.S. Ramaiah, R.D. Pilkington, A.E. Hill, R.D. Tomlinson, A.K. Bhatnagar, Mater. Chem. Phys. 68 (2001) 22–30.
[32] Y.Q. Liu, L. Gao, Mater. Chem. Phys. 91 (2005) 365–369.
[33] Z.H. Zhang, W.S. Chin, J.J. Vittal, J. Phys. Chem. B 108 (2004) 18569–18574.